Theoretical Study of Radar Polarization Parameters Obtained from Cirrus Clouds

SERGEY Y. MATROSOV*

NOAA/ERL/Wave Propagation Laboratory, Boulder, Colorado

(Manuscript received 30 April 1990, in final form 26 October 1990)

ABSTRACT

A theoretical investigation of radar polarization parameters that characterize cloud ice backscattering is presented. The parameters considered were those commonly used in radar polarimetrics such as differential reflectivity (Z_{DR}), linear depolarization ratio (LDR), circular depolarization ratio (CDR), intrinsic degree of orientation (ORTT) as well as conventional reflectivities. Experimental data on the shapes of ice crystals and their orientations are taken into account. Results suggest that prolate-shaped scatterers can be distinguished from those having oblate shapes by analyzing the depolarization ratio dependence on the elevation angle. Calculations suggest that circular polarization parameters provide stronger signals in a cross-polar channel and also show a lesser dependence on scatterer orientation in comparison with linear polarization parameters. Propagation effects do not significantly affect the polarization parameters for equivalent water contents and cloud thicknesses that are typical for cirrus clouds. Differential phase shift that might be observed in cirrus clouds is relatively small. Finally, equivalent reflectivity factors are analyzed for several ice particle types as a function of their major axis. Reflectivity dependence on particle shapes is demonstrated, and comments on the possibility of making approximate estimates of cloud particle sizes are given.

1. Introduction

Knowledge of the microphysics and structure of cirrus clouds in the upper troposphere is important for some climate investigations. The shapes and sizes of the ice particles that make up cirrus clouds have a large effect on the clouds' optical properties in different wavelength regions. The planetary albedo thus depends on cloud properties that affect the total energy budget of the earth. Cirrus clouds can also cause interference for earth–satellite communication links and affect satellite remote sensing because of differential phase shift and volume scattering. By knowing the microphysical structure of cirrus clouds, one can more accurately estimate errors in meteorological parameters obtained from satellites and in earth–satellite communication links.

Radars are powerful tools for cloud structure investigations. However, thin cirrus clouds are often "invisible" to conventional radars operating in the centimeter and decimeter wavelength regions because of cirrus clouds have relatively low reflectivities compared with cumulus clouds. The backscatter cross section of small particles increases rapidly with increasing frequency of the transmitted radar signal, so radars operating at millimeter wavelengths have an advantage over those at longer wavelengths in detecting thin clouds. Radars operating in the microwave "window" at wavelengths of 8–9 mm (Ka-band) have been used for studies of many different atmospheric phenomena (Hobbs et al. 1985; Pasqualucci et al. 1983).

Because ice crystals can have any of a large variety of nonspherical shapes, shape-sensitive polarization parameters can provide useful information about the microphysical structure of cirrus clouds. Polarization diversity radars, therefore, have great potential for cirrus clouds investigations, and that potential is examined here. This paper presents results of theoretical modeling of different Ka-band radar polarization parameters for various types of ice crystals found in cirrus clouds. Different viewing geometries and particle orientation distributions are considered.

2. Models of ice particle shapes and orientations

According to Magono and Lee (1966), the most frequent forms of ice crystals in the upper troposphere (i.e., in cirrus clouds) are plates, bullets, columns, and needles. The larger dimension of such particles generally varies from 10 μm to 1–2 mm, and these particles tend to be horizontally oriented because of aerodynamic forcing. Characteristic dependencies exist between the thickness of plates, h, and their diameter, D, and also between diameter of needles, columns or bullets, d and its length l (Pruppacher and Klett 1978). These dependencies can be expressed by the functions

* On leave from the Main Geophysical Observatory, 194018 Leningrad, 7 Karbyshev str USSR.

Corresponding author address: Dr. Sergey Y. Matrosov, Radar Meteorology Group—WPL, NOAA, Environmental Research Laboratories, 325 Broadway, Boulder, CO 80303-3328.

$$h = A \cdot D^a$$
$$d = B \cdot l^b \qquad (1)$$

where A, a, B, and b are coefficients found from experimental data. In the present work values of the coefficients are taken from Pruppacher and Klett (1978) (see Table 1).

Figure 1 depicts how the ratio of minor to major dimensions varies with the major dimension of ice particles that were chosen for modeling. This ratio diminishes with increasing size of the ice crystals. This diminishing, however, is not very distinct. In the size range of 0.2 to 1 mm for all types of ice crystals except long columns. The most deformed particles or particles with the smallest axial ratio are hexagonal plates and needles, and the least deformed are solid columns.

The common geometrical model for hydrometeors is a spheroid, the shape obtained by rotating an ellipse either around its minor axis (an oblate spheroid) or around its major axis (a prolate spheroid). Other possible models for the shapes of ice crystals are the hexagonal cylinder for plates and columns, the round cylinder for needles, and the prolate spheroid for bullets. For thick plates and columns preliminary calculations were made for two cases: one for the aforementioned particle shapes and the other for oblate and prolate spheroids with appropriate axial ratios. A perturbation approach (Morrison and Cross 1974) was used in both cases. Oblate spheroids represented both types of plates, and prolate spheroids represented the remaining crystal types. These calculations show that relative differences between polarization parameters of interest for these two cases as a rule do not exceed 5%–10%. This is smaller than the variation caused by natural uncertainties of the coefficients in Eq. (1) because of the spread in the experimental data for ice particle deformation in Pruppacher and Klett (1978). The obtained result means that spheroids can adequately represent the scattering by common ice crystal shapes.

According to results of Yeh et al. (1982) the Rayleigh approximation is generally valid in the Ka-band even for largest ice particles in cirrus clouds. Consequently, all polarization parameters presented here were computed by using the well-known Rayleigh approach (see for example Bohren and Huffman 1983) for assumed oblate and prolate spheroidal particle shapes with appropriate axial ratios.

TABLE 1. Coefficients in dimensional relationships for various ice crystal types. Particle dimensions are in centimeters. Classification according to Magono and Lee (1966).

Ice particle type	A	a	B	b
Thick plates, Clg	0.138	0.778	—	—
Hexagonal plates, Pla	0.014	0.474	—	—
Solid columns, Cle	—	—	0.578	0.958
Solid bullets, Clc	—	—	0.153	0.786
Long columns, Nle	—	—	0.035	0.437
Needles, Nla	—	—	0.031	0.611

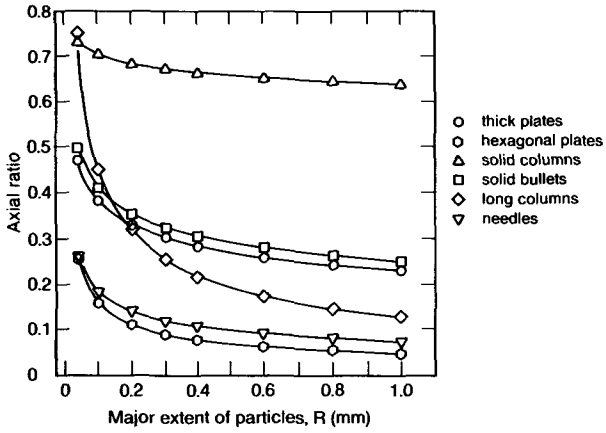

FIG. 1. Minor to major extent ratio (axial ratio) of ice crystals in cirrus clouds as a function of particle major axis.

According to Sassen (1980), ice crystals with larger dimensions greater than 0.1–0.2 mm (which usually provide the main contribution in radar echoes) tend to be horizontally oriented and their deviation from the horizontal plane is Gaussian in character. The general orientation of spheroidal particles can be described by two angular distributions of the particle's symmetry axis in a spherical coordinate system. Here it was assumed that the azimuth angle (φ) distribution was uniform and the zenith angle (θ) distribution was Gaussian with a mean value of 0° for plates and 90° for bullets, needles, and columns; i.e., the major axis was in the horizontal plane for all particles. The effects of the particle spread from the mean horizontal orientation was taken into account by considering different values of the standard deviation in the zenith angle distribution. These values varied from 0° to 45°.

3. Theoretical background

All measurable polarization information can be obtained from the four elements of the amplitude-scattering matrix **S**. This matrix gives the relationship between the electrical field components of the scattered and incident electromagnetic waves. It is convenient to consider the elements of this matrix in the linear basis of the vertical (v) and horizontal (h) polarizations. At large distances r (in comparison with the wavelength λ) for an individual particle,

$$\begin{pmatrix} E_v \\ E_h \end{pmatrix}_{(s)} \sim \frac{\exp(ikr)}{-ikr} \begin{pmatrix} s_{1,1} & s_{1,2} \\ s_{2,1} & s_{2,2} \end{pmatrix} \begin{pmatrix} E_v \\ E_h \end{pmatrix}_{(i)}, \qquad (2)$$

where (i) and (s) represent the incident and the scattered fields respectively, and k is the radar wavenumber. If the incident wave propagates along one of the principal axes of a particle, $s_{1,2} = s_{2,1} = 0$ in cases of backward and forward scattering. For arbitrary orientation of a particle, the elements of the scattering matrix **S** can be expressed in terms of scattering amplitudes along

the particle symmetry axis s_1 and a perpendicular axis s_2 (Holt 1984):

$$\mathbf{S} = \begin{pmatrix} s_1' \cos^2\alpha + s_2' \sin^2\alpha & (s_1' - s_2') \sin\alpha \cos\alpha \\ (s_1' - s_2') \sin\alpha \cos\alpha & s_2' \cos^2\alpha + s_1' \sin^2\alpha \end{pmatrix} \tag{3}$$

where

$$s_1' = s_2 \cos^2\Psi + s_1 \sin^2\Psi$$
$$s_2' = s_2. \tag{4}$$

In Eq. (3), α is the canting angle in the polarization plane, i.e., the plane perpendicular to the propagation vector of the incident wave, and Ψ is the angle between the particle symmetry axis and the incident wave propagation vector. The geometry of scattering adapted from Holt (1984) is shown in Fig. 2, where ON is the particle symmetry axis, OK is the propagation vector of the incident wave, ON′ and ON″ are projections of ON on the horizontal and polarization planes respectively. The XYZ and X′Y′Z′ coordinate systems define the particle orientation with respect to the horizontal and to the incident beam respectively. For trigonometrical functions of the above mentioned angles, which are needed to calculate the amplitude-scattering matrix elements, the following relationships are valid:

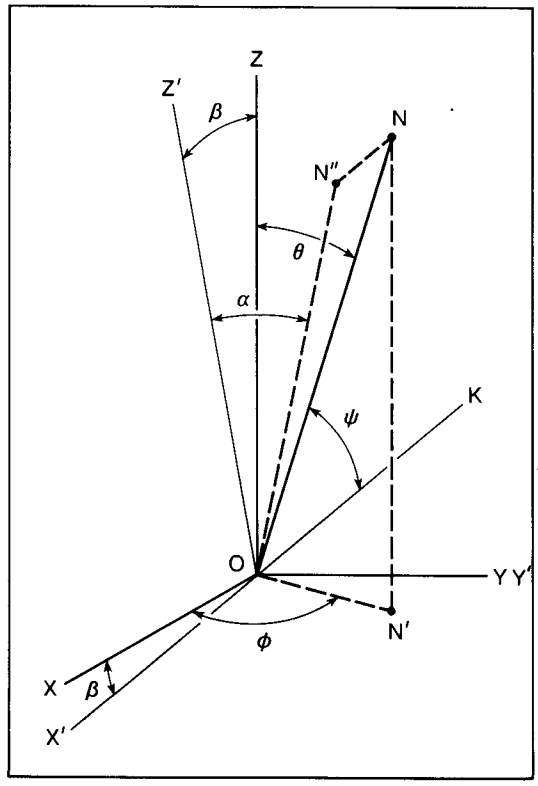

FIG. 2. The geometry of the problem.

$$\cos\alpha \sin\Psi = \cos\theta \cos\beta + \sin\theta \sin\beta \cos\varphi$$
$$\sin\alpha \sin\Psi = \sin\theta \sin\varphi$$
$$\cos\Psi = \cos\theta \sin\beta - \sin\theta \cos\beta \cos\varphi \tag{5}$$

where β is the radar elevation angle.

The matrix **S** describes scattering properties of a particle, but if there are other scatterers along the propagation path, the signals received from the illuminated volume are changed. On the radio frequencies signals are effected mostly by hydrometeors. Round-trip propagation effects (when inner volumes of clouds are studied) can be taken into account by considering the matrix **L** instead of the matrix **S**:

$$\mathbf{L} = \mathbf{I} \cdot \mathbf{T}(\bar{\alpha}) \cdot \mathbf{U} \cdot \mathbf{T}(-\bar{\alpha}) \cdot \mathbf{I} \cdot \mathbf{S} \cdot \mathbf{T}(-\bar{\alpha}) \cdot \mathbf{U} \cdot \mathbf{T}(\bar{\alpha}) \tag{6}$$

where **T** and **U** are rotation and propagation matrices, respectively. And $\bar{\alpha}$ is the mean canting angle in the polarization plane of particles on the propagation path.

Products of matrixes $\mathbf{T}(-\bar{\alpha}) \cdot \mathbf{U} \cdot \mathbf{T}(\bar{\alpha})$ and $\mathbf{T}(\bar{\alpha}) \cdot \mathbf{U} \cdot \mathbf{T}(-\bar{\alpha})$ describe radar signal propagation to the illuminated volume and back respectively, and matrix **I** describes the coordinate system inversion due to backscattering. Matrixes **T** and **I** are written as follows:

$$\mathbf{T}(\alpha) = \begin{pmatrix} \cos\alpha & \sin\alpha \\ -\sin\alpha & \cos\alpha \end{pmatrix}$$
$$\mathbf{I} = \begin{pmatrix} 1 & 0 \\ 0 & -1 \end{pmatrix}. \tag{7}$$

It was assumed that $\bar{\alpha}$ has the same value along the entire path. If a coordinate system is applied where scatterers are distributed symmetrically, i.e., $\bar{\alpha} = 0$, (achieved by using the rotation matrix **T**), the propagation matrix U is diagonal (Oguchi 1983) and its elements can be expressed as follows:

$$u_{j,j} = \exp(-2\pi r_o f_{j,j}/k^2) \quad (j = 1, 2), \tag{8}$$

where r_o is the one-way propagation path length. The values of $f_{j,j}$ ($j = 1, 2$), which are related to the wave propagation constants, can be calculated from

$$f_{j,j} = 0.5 \int_0^{R_{\max}} N(R) s_j(R) [\exp(-2\sigma_1^2)$$
$$\times \cos(2\bar{\gamma}) + 1] \exp(-2\sigma_2^2) dR, \tag{9}$$

where $N(R)$ is the particle-size distribution function in terms of the crystal large dimension (R), $\bar{\gamma}$ is the mean angle between the particle symmetry axes and their projections on the polarization plane, σ_2 and σ_1 are the standard deviations of α and γ, respectively, and $s_j(R)$ is a diagonal element of the amplitude-scattering matrix along a principal axis for forward scattering. In the Rayleigh region, **S** matrix elements for forward and backscattering have the same value. Further, it was assumed that the orientation and microphysical properties of the particles in the illuminated

volume and along the propagation path are the same. In Eq. (9), the propagation constant for free space is omitted because differential effects are of main interest. Differential attenuation described by absolute values of the diagonal elements [Eq. (8)] is negligibly small in ice clouds, and practically all propagation effects are due to phase rotation.

Trigonometrical functions of angle γ which are needed to calculate the propagation matrix elements can be obtained from trigonometrical functions of angles α, θ, φ, β. The relationships are very simple for $\beta = 0$

$$\sin\gamma = \sin\theta\cos\varphi$$
$$\cos\gamma\sin\alpha = \sin\theta\sin\varphi \qquad (10)$$

when $\beta \neq 0$, corresponding relationships can be found by transforming the original spherical coordinate system to one where the v-polarization unit vector is vertical.

The matrix $\mathbf{L}$ given in Eq. (6) describes backscattering of a plane electromagnetic wave, taking into account the propagation effects. It is more convenient to obtain the radar parameters in the linear basis (v–h) and then transform the results to other bases, e.g., circular. In the linear system, we consider reflectivities in the main (horizontal and vertical) and orthogonal channels (Z_h, Z_v, $Z_{h,v}$) differential reflectivity (Z_{DR}), linear depolarization ratio (LDR), and a correlation coefficient between the copolar and cross-polar components (W_L):

$$Z_h \equiv X\int_0^{R_{max}}\int_\Omega |I_{2,2}(R)|^2 N(R)G(\theta,\varphi)dR\alpha\Omega$$
$$Z_v \equiv X\int_0^{R_{max}}\int_\Omega |I_{1,1}(R)|^2 N(R)G(\theta,\varphi)dR\alpha\Omega$$
$$Z_{h,v} \equiv X\int_0^{R_{max}}\int_\Omega |I_{2,1}(R)|^2 N(R)G(\theta,\varphi)dR\alpha\Omega$$
$$W_L \equiv X\int_0^{R_{max}}\int_\Omega I_{2,1}(R)I^*_{1,1}(R)\cdot N(R)G(\theta,\varphi)dR\alpha\Omega$$
$$Z_{DR} \equiv 10\log_{10}(Z_h/Z_v)$$
$$LDR \equiv 10\log_{10}(Z_{h,v}/Z_h) \qquad (11)$$
$$X = \frac{\lambda^6}{\pi^6}|(m^2+2)/(m^2-1)|^2 \qquad (12)$$

where $*$ is the complex conjugation sign, G is the particle orientation distribution function, m is the complex refractive index for ice, and Ω is a solid angle. Function G is the superposition of the azimuth and zenith angle distribution functions which were described above.

Radar parameters in right-hand circular (RHC) and left-hand circular (LHC) polarizations can be obtained from elements of the amplitude-scattering matrix:

$$\mathbf{C} = \mathbf{Y}^{-1}\cdot\mathbf{L}\cdot\mathbf{Y} \qquad (13)$$

where

$$\mathbf{Y} = \frac{1}{\sqrt{2}}\begin{vmatrix} i & -i \\ 1 & 1 \end{vmatrix}. \qquad (14)$$

Circular polarization parameters of interest are reflectivities in both main and orthogonal channels (W_m and W_o), the circular depolarization ratio (CDR), and the correlation coefficient between the two components (W_c). These quantities are

$$W_m \equiv X\int_0^{R_{max}}\int_\Omega |c_{1,2}(R)|^2 N(R)G(\theta,\varphi)dR\alpha\Omega,$$
$$W_o \equiv X\int_0^{R_{max}}\int_\Omega |c_{2,2}(R)|^2 N(R)G(\theta,\varphi)dR\alpha\Omega,$$
$$CDR \equiv 10\log_{10}(W_o/W_m),$$
$$W_c \equiv X\int_0^{R_{max}}\int_\Omega c^*_{1,2}(R)\,c_{2,2}(R)N(R)G(\theta,\varphi)dR\alpha\Omega. \qquad (15)$$

It was assumed, without losing generality, that the left-hand circularly polarized wave is transmitted. It is often more convenient to consider the normalized correlation coefficient between reflected radar signals in different polarization channels. Here the definition given by McCormick and Hendry (1975) for the normalized correlation coefficient in the circular basis (ORTT) was adopted and a similar definition for the linear basis ($ORTT_L$) was assumed:

$$ORTT = |W_c|/\sqrt{(W_oW_m)}$$
$$ORTT_L = |W_L|/\sqrt{(Z_vZ_{h,v})}. \qquad (16)$$

Characteristics presented in Eqs. (11) and (15) can be measured by radars transmitting either a linear [Eq. (11)] or a circular [Eq. (15)] polarized electromagnetic wave and using two receivers, one for co-polar and the other for cross-polar components of reflected signals. For accurate Z_{DR} measurements, pulse-to-pulse polarization switching of the transmitted signal is also required.

Theoretical modeling of the above parameters was carried out for ice particles. Bulk density of ice for various crystal types of different sizes were taken from Pruppacher and Klett (1980); data of the complex refractive index for ice at different densities were taken from Rozenberg (1972). These data show the almost linear decrease of the real parts of the complex refractive indices from 1.78 for the ice density $\rho = 0.916$ g cm^{-3} to 1.38 for $\rho = 0.46$ g cm^{-3}. Imaginary parts of these indices are usually very small and do not affect the backscattering properties of ice particles significantly.

4. Results

a. Scope of the calculations

The four polarization parameters and main-channel radar reflectivity discussed earlier were computed and plotted in Figs. 3 through 9. The polarization parameters plotted are LDR, CDR, ORTT, and Z_{DR}. In these calculations, the incident wavelength was 8.6 mm, and ice particle types often found in cirrus clouds were modeled as oblate and prolate spheroids with size-dependent axial ratios specified by Pruppacher and Klett (1978) and expressed in Eq. (1). Figures 5–6 also illustrate how the computed parameters depend on the radar elevation angle.

All polarization results given here are for ice particles with a major axis of 0.2 mm because other calculations, not shown here, indicate that LDR and CDR vary less than about 2 dB for all particle types in the size range from 0.08 mm to 1 mm. Here Z_{DR} varied less than 0.5 dB for all particle types except long columns, which showed a 0.5 to 0.7 dB variation over this rather large range of sizes. ORTT showed practically no variation with size over this range. Because of the weak dependency of these polarization parameters with size in this range, and also because of the uncertainty of particle size distributions within cirrus clouds, a monodisperse distribution at 0.2 mm was chosen. Particles smaller than 0.08 mm tend to be masked by the presence of a few bigger ones within the radar resolution cell, and particles larger than 1 mm tend to precipitate out of the cloud.

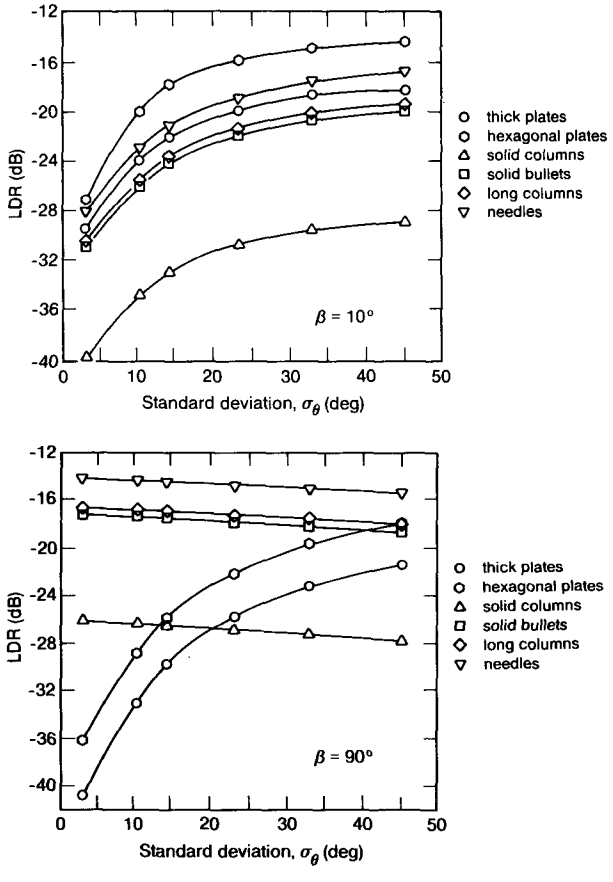

FIG. 3. Linear depolarization ratio dependence on the standard deviation (σ_θ) of particle orientation from the horizontal orientation for different types of ice crystals with D = 0.2 mm: (a) radar elevation angle β = 10° and (b) radar elevation angle β = 90°.

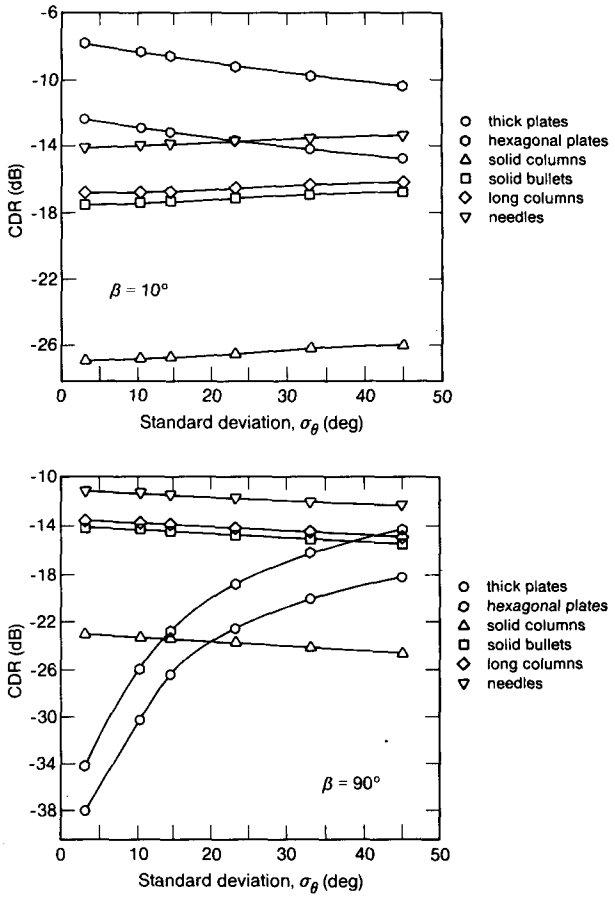

FIG. 4. Same as Fig. 2, but showing circular depolarization ratio.

b. LDR and CDR signatures

Figures 3 and 4 depict LDR and CDR as functions of the standard deviation of the symmetry axes zenith angle (σ_θ). When σ_θ = 0°, for example, major axes of all the particles are in the horizontal plane. LDR values are very small for all types of scatterers when they do not deviate from horizontal orientation significantly and are observed at a low elevation angle (10°). These values for ice plates remain small for a large radar elevation angle, as Fig. 2b illustrates. LDR values for prolates with $\sigma_\theta \leq 15°$ are greater than those for oblates observed at vertical incidence (β = 90°). Also, at vertical incidence, LDR differences between oblates

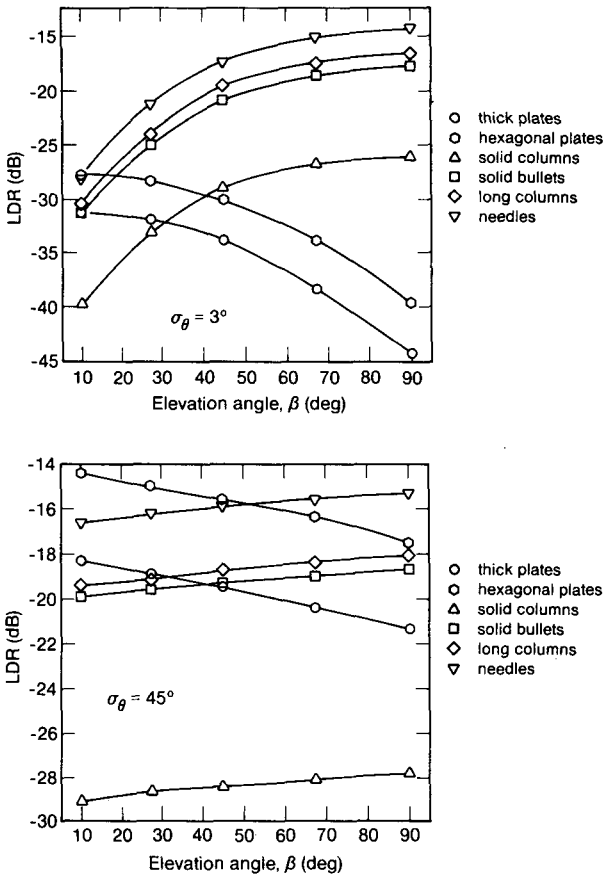

FIG. 5. Linear depolarization ratio as a function of the radar elevation angle for different types of ice crystals with standard deviation of particles from horizontal orientation: (a) $\sigma_\theta = 3°$, (b) $\sigma_\theta = 45°$.

(plates) and prolates (columns, bullets, needles) become less distinct for large σ_θ.

The CDR behavior at vertical incidence is similar to that of LDR but the CDR values tend to be 3–4 dB higher. However, at the low elevation shown in Fig. 3a, CDR can be as much as 10 dB greater than LDR. Unlike LDR, CDR does not tend to be very small for horizontally oriented scatterers. It can be seen also that except for oblate particles, the CDR is somewhat independent on σ_θ when observed at vertical incidence. Radar signals from cirrus clouds are usually quite weak, and the signal strength of the cross-polar component is sometimes lower than the detectable threshold signal. Because the CDR produces a stronger cross-polar signal than does LDR, circular polarization has an advantage when clouds with low reflectivities are studied.

Figures 3 and 4 show that, for the zenith-looking geometry, oblate scatterers can be distinguished from prolates only if the particle deviation from horizontal orientation is not significant. As it will be shown later, some information about the common degree of particle orientation can be obtained from the ORTT measurements. CDR (or LDR) values of ice solid columns are much lower than those for other types of prolate scatterers because the deformation of this type of ice crystal is not large (see Fig. 1). These CDR values do not depend significantly on σ_θ and are generally in the region from −23 to −27 dB for all elevation angles; LDR values can be much lower, especially at low elevation angles.

Figures 5 and 6 show the variation of LDR and CDR on the radar elevation angle. Variations with elevation angle for oblate and prolate scatterers are quite different which suggests a means for distinguishing between them. Curves for oblate particles show a decrease in CDR when the radar elevation angle increases. Prolate particles show a reverse tendency. Therefore, it should be possible to distinguish between prolate and oblate types of scatterers in horizontally homogeneous clouds by using range–height-indicator (RHI) scanning at fixed azimuth. Scanning 30° or 40° from zenith should be sufficient to detect the general tendency of the angular CDR or LDR dependence, especially for small σ_θ.

A qualitative estimate of the particle axial ratio for prolate particles can be obtained from CDR measurements. That is, the mean CDR values of such particles decrease from approximately −12 dB for scatterers with

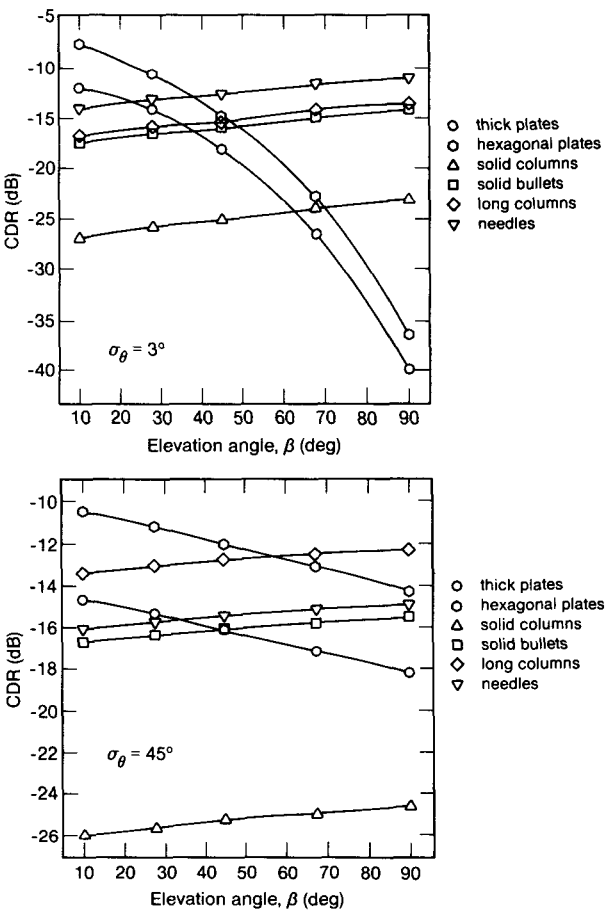

FIG. 6. Same as Fig. 4, but showing circular depolarization ratio.

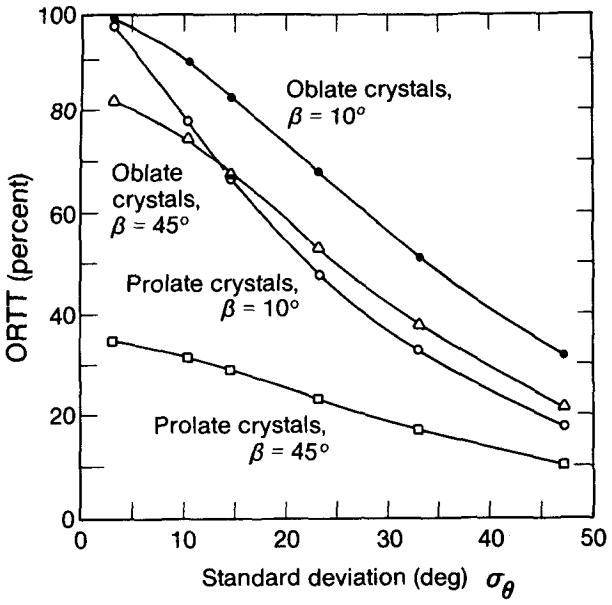

FIG. 7. ORTT dependence of oblate and prolate scatterers on particle deviation from horizontal orientation for different viewing geometries.

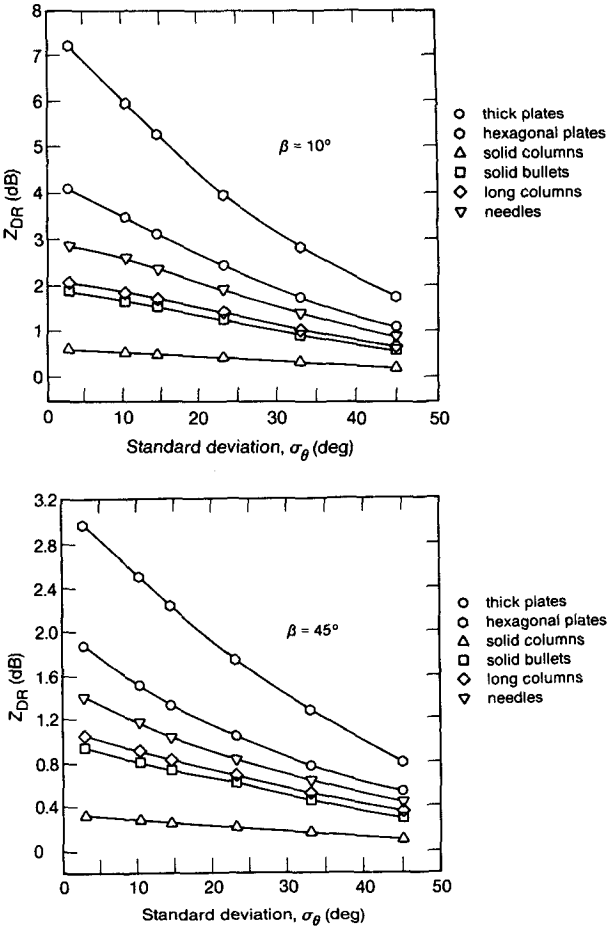

FIG. 8. Differential reflectivity dependence on the standard deviation (σ_θ) of particle orientation from horizontal orientation for different types of ice crystals: (a) radar elevation angle $\beta = 10°$ and (b) radar elevation angle $\beta = 45°$.

a high degree of deformation, e.g., needles that have an axial ratio of about 0.1, to 12–14 dB smaller for scatterers with a relatively low degree of deformation, such as columns with an axial ratio of about 0.7. These mean values are fairly independent on the particle orientation. It is more difficult to evaluate the degree of deformation for oblates because mean CDR values for oblates are influenced by the radar elevation angle and particle orientation.

Results presented above are for solid ice spheroids. To estimate the effect of hollow cores sometimes found in natural ice crystals, we assumed that the particle bulk density is diminished by 25% from the values given in (Pruppacher and Klett 1978). Diminishing the ice bulk density decreases CDR and LDR values, but not by more than 2–2.5 dB. This suggests that the previous conclusions for solid ice crystals are also valid for hollow crystals.

As mentioned before, parameters measured by polarization diversity radars can suffer effects of propagation through an anisotropic medium. Results presented above represent intrinsic scattering properties exclusive of propagation effects. To evaluate propagation effects, we made calculations with r_o in Eq. (8) set to 2 km rather than zero. This value is sufficiently large because real cirrus clouds are rather thin. The monodisperse function $N(R)$ in Eq. (9) was chosen for this modeling to constrain the effective cloud ice water content to be equal to 0.1 g m^{-3}, a value somewhat greater than the average for cirrus clouds. It is clear that the most significant propagation effects can occur when all particles along the path have their major dimensions in the horizontal plane and are observed at low elevation. These conditions were selected to provide an upper limit on effects caused by propagation.

Results obtained for this case ($\beta = 10°$) showed that propagation effects had a negligibly small influence on

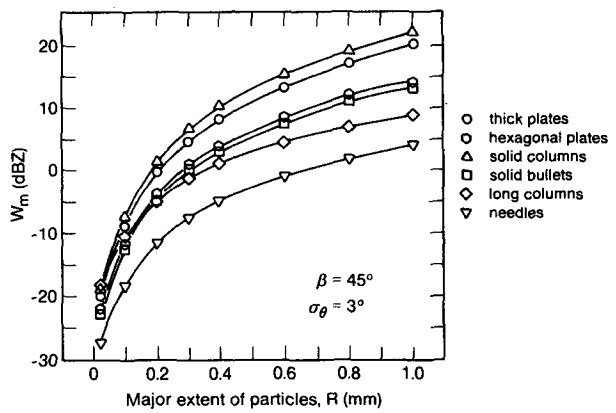

FIG. 9. Radar reflectivity on circular polarization (the main channel) as a function of major extent of ice crystals. Equivalent cloud ice water content is 0.1 g m^{-3}.

the LDR and CDR parameters. These parameters tend to increase very slightly because of these effects, but their changes do not as a rule exceed 0.2–0.3 dB for all the types of ice crystals considered here. Given these results, propagation effects can safely be ignored when investigating cirrus clouds with radar. However, this conclusion may not be valid when cirrus anvils of large cumulus clouds are observed and radar signals propagate through long paths containing large hydrometors at high concentrations.

c. ORTT signatures

The ORTT and ORTT_L, parameters are strongly dependent on the degree of hydrometeor orientation. ORTT dependence on orientation parameters and on the radar elevation angle are similar for the two kinds of ice plates considered here. This is also true for the four types of prolates. Consequently, only averages of ORTT for the two types of particle, oblates and prolates, are shown in Fig. 7. The variation of ORTT with σ_θ is shown for prolates and oblates only for 10° and 45° elevations because no variation is expected when zenith-looking geometry is used.

Figure 7 shows that ORTT coefficients are a satisfactory indicator of the common degree of orientation for oblate particles over a wide range of elevation angles. If it is known (for example, from CDR measurements) that the cloud contains mostly oblate scatterers, a measure of their deviation from the mean orientation can be estimated. Unfortunately, this result does not seem to be valid for a wide range of elevation angles which is the case for prolate crystals. In this situation, estimates can be made only for low elevation angles. Given this result, along with the conclusion that propagation effects are small, it seems more appropriate to measure radar polarization of cirrus clouds at low elevation angles. However, signal-to-noise considerations may dictate otherwise and require that close-range, high-elevation measurements be taken. It should be mentioned that zenith-viewing ORTT estimates could provide information about the nonuniformity of azimuth angle distribution of the scatterer axes.

ORTT_L values were computed but are not presented here because ORTT better reflects particle orientation characteristics. The propagation effects do not cause any significant changes in the ORTT coefficients.

d. Z_{DR} signatures

Polarization diversity radars transmitting linearly polarized signals can produce not only depolarization ratio data (LDR) but also differential reflectivity data (Z_{DR}) if pulse-to-pulse polarization switching is used. In Fig. 8, the variation of Z_{DR} with σ_θ is plotted for the six ice crystal types observed at two different elevation angles. Z_{DR} is zero when zenith-looking geometry is used due to the assumed uniform azimuth angle distribution. For low elevations Z_{DR} can be as high as 7–8 dB. Such high values of differential reflectivity were observed when studying ice clouds with radar (Sassen et al. 1989).

It can be seen in Figs. 8a and 8b that oblate ice particles (i.e., plates) have greater Z_{DR} than prolate particles by as much as 4 dB. The largest differences are seen if all the particles are in the horizontal plane (small σ_θ) and if clouds are viewed from low elevation angles. Differential reflectivities of oblates can be greater than 3 dB, but for prolates they never exceed this value.

The Z_{DR} decreases when the radar elevation angle increases for the ice scatterers considered here. Increased particle deviation from horizontal orientation also reduces Z_{DR}. This suggests that it could be possible to distinguish between plates and prolates if the particles do not deviate significantly from horizontal orientation.

For the general case Z_{DR} data depend on both particle shape and orientation and do not provide much more additional information than depolarization measurements about ice scatterers in cirrus clouds. However, these data can indicate either horizontal or vertical preferable orientation of particle major dimensions. In vertical orientation, Z_{DR} values would be negative.

e. Differential phase shift estimation

Although propagation effects (which are caused mostly by phase rotation) are small in cirrus clouds, it is of interest to estimate differential phase shift (DPS) between horizontally and vertically polarized electromagnetic waves. DPS can cause "cross-talk" between RHC and LHC polarization channels used in earth-satellite communication links. It also can be used to study denser clouds. DPS accumulates along the propagation path and depends on the concentration of scatterers and their orientations. It can be calculated from

$$\mathrm{DPS} = \frac{\lambda^2}{2\pi}\int_0^{R_{\max}}\int_\Omega \mathrm{Im}(s_{2,2} - s_{1,1}) \times N(R)G(\theta, \varphi)\,dR\alpha\Omega \quad (17)$$

where $s_{1,1}$ and $s_{2,2}$ are elements of the matrix **S** given in Eq. (3). McCormick and Hendry (1979) suggested estimating DPS between two radar resolution cells in a hydrometer medium by differences of the imaginary part of the complex ratio W_c/W_m. Results obtained here for low elevation angles show a linear relationship between DPS and $\Delta\,\mathrm{Im}(W_c/W_m)$:

$$\mathrm{DPS} = K\Delta\,\mathrm{Im}(W_c/W_m). \quad (18)$$

The factor K is approximately 1.1–1.2 for the ice particles considered here.

The imaginary parts of the W_c/W_m ratios are small for ice particle concentrations that occur in cirrus clouds. Differences of $\mathrm{Im}(W_c/W_m)$ are also expected to be small because of the short propagation paths that would result from these clouds, making DPS measurements difficult to obtain.

f. Reflectivity signatures

Although polarization parameters do not depend significantly on particles sizes, it is known that conventional radar reflectivity is strongly dependent on the scatterer size. Reflectivities for the vertical and horizontal polarizations (Z_v and Z_h) also depend on the scatterer orientations rather strongly. However, the main channel reflectivity in the circular basis (W_m) does not depend greatly on particle orientation. Increasing the radar elevation angles also does not cause significant changes in W_m.

Figure 9 shows m as a function of the particle long dimension for different types of ice particles. It was assumed that the radar resolution cell was uniformly filled with scatterers of the same size. As before, the concentration of particles was chosen such that the cloud ice water content was equal to 0.1 g m^{-3}. W_m values were computed for an elevation angle of 45° and for $\sigma_\theta = 3°$. For all the other elevation angles between 10° and 90° and for $3° < \sigma_\theta < 45°$, W_m was found to differ from the values presented in Fig. 8 by less than 0.7 dBZ for prolate particles and 2.0 dBZ for oblate particles. The least deformed particles, solid columns, show the strongest backscattered signal.

For some climate study applications, it is important to estimate (even approximately) the mean size of cirrus cloud particles that can affect the radiation energy budget of the earth. An accurate estimate using only single-wavelength polarization data seems to be impossible because polarization parameters do not show significant dependence on scatterer sizes and reflectivities depend on both particle size and concentration. But it should be mentioned that in the Rayleigh region the former dependence is much stronger than the latter one. This means that one can roughly estimate the size of particles that contribute to the scattered signal most of all if the value for equivalent cloud water content (i.e., the particle concentration) is assumed. This value can be adopted, for example, from climatological data.

5. Conclusions

In this paper we have examined in theory the polarization parameters of radar signals reflected by ice clouds. Different particle types were considered. The circular polarization is preferred to linear because of the more powerful backscattering signals in the orthogonal polarization channel. In addition, CDR is less influenced by the orientation of scatterers than is LDR. By analyzing the elevation angle dependence of depolarization, one can distinguish between prolate and oblate types of hydrometeors in the illuminated volume. An average axial ratio of the scatterers can also be roughly evaluated. Measuring the correlation coefficient between signals in the main and orthogonal channels provides information on particle deviation from mean orientation. A very approximate estimate of particle size can also be made from circular reflectivity data, but only with an assumed value of equivalent cloud water content and an assumed monodisperse size distribution. It was also shown that propagation effects in thin ice clouds are small.

These results show that polarization diversity radars can provide useful information about ice particles in cirrus clouds. Extensive experimental investigations are being planned with recently upgraded WPL Ka-band radar. This radar has a unique offset Cassegrain antenna designed especially for precise polarization measurement in ice clouds (Kropfli et al.) 1990).

Acknowledgments. This work was done while the author held a National Research Council Associateship in the NOAA Wave Propagation Laboratory. Special thanks are due to R. A. Kropfli for helpful conversations and constructive review of this manuscript. Discussions with W. L. Eberhard are also acknowledged.

REFERENCES

Bohren, C. F., and D. R. Huffman, 1983: *Absorption and Scattering of Light by Small Particles.* John Wiley and Sons, 530 pp.

Hobbs, P. V., N. T. Funk, R. R. Weis, J. D. Locatelli and K. R. Biswas, 1985: Evaluation of a 35 GHz radar for cloud physics research. *J. Oceanic Atmos. Technol.,* **22,** 35–48.

Holt, A. R., 1984: Some factors affecting the remote sensing of rain by polarization diversity radar in the 3- to 35-GHz frequency range. *Radio Sci.,* **19,** 1399–1421.

Kropfli, R. A., B. W. Bartram and S. Y. Matrosov, 1990: The upgraded WPL dual-polarization 8-mm wavelength Doppler radar for microphysical and climate research. Preprints, *AMS Conference on Cloud Physics,* San Francisco, 341–345.

Magono, C., and C. W. Lee, 1966: Meteorological classification of natural snow crystals. J. Fac. Sci., Hokkaido University, Ser. 7, 2, No. 4, 321–335.

McCormick, G. C., and A. Hendry, 1975: Principles for the radar determination of the polarization properties of precipitation. *Radio Sci.,* **10,** 431–434.

——, and ——, 1979: Radar measurements of precipitation-related depolarization in thunderstorms. *IEEE Trans.,* **GE-17,** No. 4, 142–150.

Morrison, J. A., and M. J. Cross, 1979: Scattering of a plane electromagnetic wave by axisymmetric raindrops. *Bell System Tech. J.,* **53,** 955–1019.

Oguchi, T., 1983: Electromagnetic wave propagation and scattering in rain and other hydrometeors. *Proc. IEEE,* **71,** 1029–1078.

Pasqualucci, F., B. W. Bartram, R. A. Kropfli and W. R. Moniger, 1983: A millimeter wavelength dual-polarization Doppler radar. *J. Climate Appl. Meteor.,* **22,** 758–765.

Pruppacher, H. R., and J. D. Klett, 1978: *Microphysics of Clouds and Precipitation.* D. Reidel 714 pp.

Rozenberg, V. I., 1972: *Scattering and Extinction of Electromagnetic Waves by Atmospheric Particles.* Leningrad, Gidrometeoizdat, 348 pp.

Sassen, K., 1980: Remote sensing of planar ice crystal fall attitudes. *J. Meteor. Soc. Japan,* **58**(5), 422–429.

——, D. O'C. Starr and T. Uttal, 1989: Mesoscale and microscale structure of cirrus clouds: three case studies. *J. Atmos. Sci.,* **46**(3), 371–396.

Yeh, C., R. Woo, A. Ishimary and J. Armstrong, 1982: Scattering by single ice needles and plates at 30 GHz. *Radio Sci.,* **17**(6), 1503–1510.